




Article

Multibeam Characteristics of a Negative Refractive Index Shaped Lens

Salbiah Ab Hamid ^{1,*}, Nurul Huda Abd Rahman ^{1,*} , Yoshihide Yamada ², Phan Van Hung ³ 
and Dinh Nguyen Quoc ³ 

¹ Faculty of Electrical Engineering, Universiti Teknologi MARA, Shah Alam 40450, Selangor, Malaysia

² Malaysia-Japan International Institute of Technology, Universiti Teknologi Malaysia, Kuala Lumpur 54100, Malaysia; yoshihide@utm.my

³ Faculty of Radio Electronic Engineering, Le Quy Don Technical University, Hanoi City 100000, Vietnam; phanvanhung@tcu.edu.vn (P.V.H.); dinhngq@mta.edu.vn (D.N.Q.)

* Correspondence: 2014365251@isiswa.uitm.edu.my (S.A.H.); nurulhuda0340@uitm.edu.my (N.H.A.R.)

Received: 22 August 2020; Accepted: 2 October 2020; Published: 7 October 2020



Abstract: Narrow beam width, higher gain and multibeam characteristics are demanded in 5G technology. Array antennas that are utilized in the existing mobile base stations have many drawbacks when operating at upper 5G frequency bands. For example, due to the high frequency operation, the antenna elements become smaller and thus, in order to provide higher gain, more antenna elements and arrays are required, which will cause the feeding network design to be more complex. The lens antenna is one of the potential candidates to replace the current structure in mobile base station. Therefore, a negative refractive index shaped lens is proposed to provide high gain and narrow beamwidth using energy conservation and Abbe's sine principle. The aim of this study is to investigate the multibeam characteristics of a negative refractive index shaped lens in mobile base station applications. In this paper, the feed positions for the multibeam are selected on the circle from the center of the lens and the accuracy of the feed position is validated through Electromagnetic (EM) simulation. Based on the analysis performed in this study, a negative refractive index shaped lens with a smaller radius and slender lens than the conventional lens is designed, with the additional capability of performing wide-angle beam scanning.

Keywords: lens antenna; negative refractive index; multibeam; beam scanning

1. Introduction

In recent years, there has been a rapid development of antennas to meet the advanced mobile technology requirements. In the 5G mobile technology system, millimeter wave is used, which produces a smaller cell size and requires a multibeam radiation pattern in order to achieve massive Multiple Input Multiple Output (MIMO) operation [1,2] with the purpose to serve massive number of users, consistent interconnectivity and larger capacity. At millimeter wave, the base station size becomes less than 30cm. So, aperture antennas such as reflector antennas and dielectric lens antennas become promising candidates as compared to the present array antennas. For multibeam operation, the dielectric lens antenna can achieve very good performance by designing the lens using Abbe's sine condition [3], which is validated further in this paper.

There were several studies conducted to investigate the multibeam application using the lens antenna. The Luneburg lens antenna is one of the commonly used designs. However, major issues of the conventional Luneburg lens are large and heavy. In [4], a Luneburg lens with an operating frequency of 1–8 GHz was proposed. In the paper, multilayer Luneburg lenses were fabricated with the diameters of 0.6 and 1.0 m and weighing of 5 and 21 kg, respectively. A number of feed antennas

was placed around the lens to produce multibeam with the same beam shapes. Beam scanning was achieved by switching the feed around the surface of the lens. The traditional Luneburg lenses weight has been reduced up to 8–10 times; however, in 5G base station application, this weight and size are not practical. A flat Luneburg lens antenna with a geometry of $80 \times 5 \text{ mm}^2$ was designed to operate at Ka-band [5]. A linear antenna array with 11 E-shaped patch antenna elements is employed to feed the lens antenna. The lens is formed by rectangular shaped concentric six layered dielectric materials with a permittivity ranging from 1.74 to 10 to achieve higher aperture efficiency. This lens antenna produces a realized gain of 14.2 dBi. In total, 11 beams are produced for $\pm 60^\circ$ beam scanning. However, a lens antenna employing natural dielectric material is known to produce a thicker lens size, and thus is not suitable for base station application. In order to reduce the lens thickness, a metamaterial lens concept was proposed [6]. Lens structure became concave and reduced the lens thickness. As for metamaterial lens fabrication, a lens of refractive index of $n = -1$ was shown in [7]. The structure is obtained by using 100 unit cells of dielectric resonator structure, 0.5 of f/D with lens aperture of 5.7λ (156 mm) at an 11 GHz operating frequency. The achieved multibeam radiation pattern is shown in [8]. To achieve a good multibeam characteristic, Abbe's sine condition design is proposed in this paper, and comparison with the energy conservation technique is analyzed.

In this paper, the application of Abbe's sine design and energy conservation design are employed to develop a metamaterial lens. Based on the lens shaping equation, the possibility of the negative refractive index design is ensured. In order to solve the design equations, a MATLAB program is developed. The design accuracies of the MATLAB program are estimated using ray tracing results and calculation of the refraction angles on the lens surfaces. For validation, the multibeam radiation pattern is calculated using a commercial electromagnetic simulator, High Frequency Structure Simulator (HFSS). Figure 1 shows the proposed base station structure.

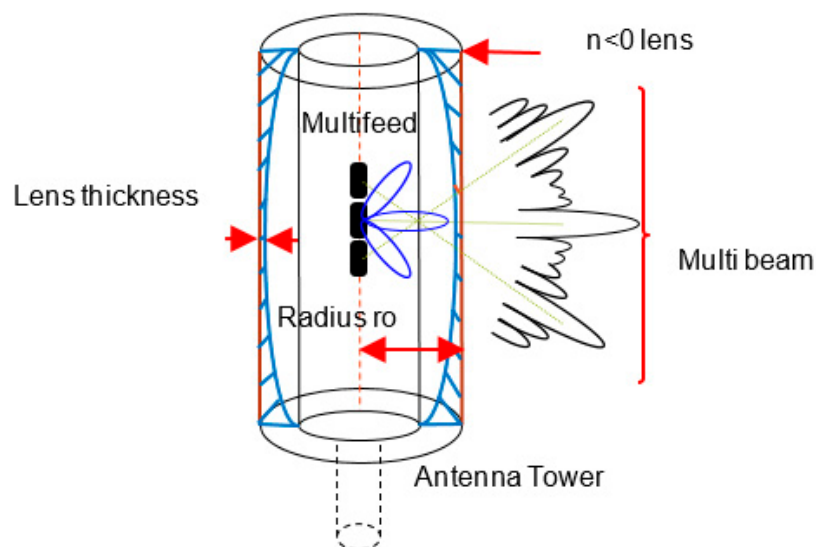


Figure 1. Proposed mobile base station structure.

2. Design Method

In designing the lens surface, the ray tracing method was employed. All rays passing through the aperture plane are designed to be parallel to the z-axis in order to achieve a flat wave front at the aperture plane.

2.1. Lens Configuration

Figure 2 shows the proposed antenna configuration and the associated radiation parameters. The feed radiator radiates signal towards the negative refractive index shaped lens, and the result is observed at the aperture. The detailed description of the parameters is shown in Table 1.

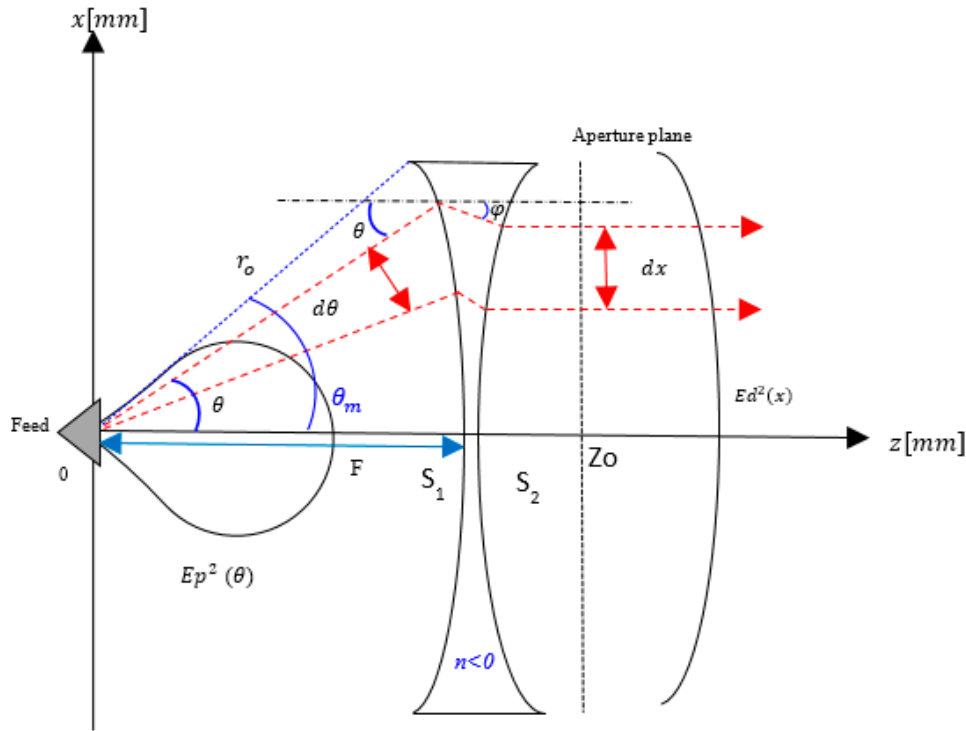


Figure 2. Lens configuration and parameters.

Table 1. Antenna parameters.

Parameter	Description
n	Refractive index
$Ep^2(\theta)$	Feed pattern
$Ed^2(x)$	Aperture Distribution
θ_m	Angle from feed to the lens edge

2.2. Lens Shape Equations

2.2.1. Aperture Distribution Designing

Based on Figure 2, at surface 1, S_1 of the lens, Snell's law is given by Equation (1) [9].

$$\frac{dr}{d\theta} = \frac{r \sin(\theta - \varphi)}{n \cos(\theta - \varphi) - 1} \tag{1}$$

At the lens surface 2, the expression for the slope $\frac{dz}{dx}$ can be derived from the condition that all exit rays after refraction are parallel to the z- axis, as shown in Equation (2). The $\frac{dz}{dx}$ expression can be separated into $\frac{dz}{d\theta}$ and $\frac{dx}{d\theta}$, as shown in Equation (2) for variable change from dx to $d\theta$.

$$\frac{dz}{dx} = \frac{n \sin(\varphi)}{1 - n \cos(\varphi)} \frac{dz}{d\theta} = \frac{n \sin(\varphi)}{1 - n \cos(\varphi)} \frac{dx}{d\theta} \tag{2}$$

The equal condition of ray path length can be expressed in Equation (3) where Lt indicates the total path length from the feed to the aperture plane.

$$Lt = r + n\left(\frac{x - r\cos\varphi}{\cos\varphi}\right) + z_0 - z = \text{constant} \tag{3}$$

By using this equation, the variable φ in Equations (1) and (2) can be expressed by the variable θ . Then, through simplification, the variable of Equations (1) and (2) becomes only θ . The electric power conservation at the ray is composed of dx and $d\theta$

$$\frac{dx}{d\theta} = \frac{Ep^2(\theta)}{\int_0^{\theta_m} Ep^2(\theta)d\theta} \frac{\int_0^{X_m} Ed^2(x)dx}{Ed^2(x)} \tag{4}$$

The three differential Equations (1), (2) and (4) determine the lens shape in the MATLAB program. For the electric field intensity at feed radiator, $Ep^2(\theta)$, Equation (5) is implemented. Meanwhile, Equation (6) is used for aperture illumination distribution, $Ed^2(x)$.

$$Ep^2(\theta) = \cos^m(\theta) \tag{5}$$

$$Ed^2(x) = \left[1 - \left(1 - \frac{1}{C}\right)\left(\frac{x}{X_m}\right)^2\right]^P \tag{6}$$

2.2.2. Abbe’s Sine Condition

In optic, a collimating lens can be designed to be a coma free for a limited scan by imposing the Abbe’s sine condition. Coma refers to the aberration inherent to certain optical designs or due to imperfection in the lens or other components that results in off-axis point sources. This condition is automatically fulfilled if the inner surface of a conventional waveguide lens is spherical. The condition in the red circle in Figure 3 interprets the Abbe’s sine condition. When the initial and the final ray are extended, these rays are intersecting inside the lens on a circle radius of f_e [2]. Abbe’s sine law in Equations (7) and (9) are applied in the MATLAB program to design the shaped lens.

$$x = f_e \sin(\theta - d\theta) \tag{7}$$

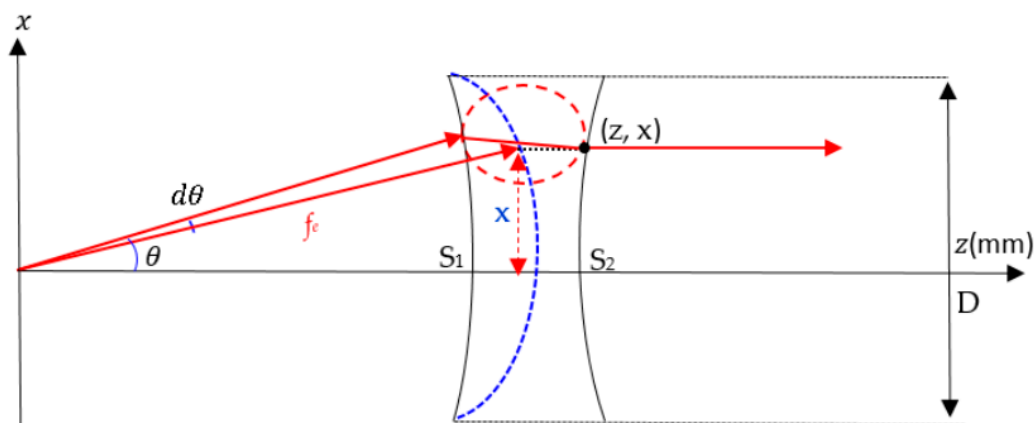


Figure 3. Abbe’s sine condition.

For $d\theta \ll 1$, Equation (7) becomes

$$x = f_e \sin\theta \tag{8}$$

$$\frac{dx}{d\theta} = f_e \cos\theta \tag{9}$$

2.3. Program Flow Chart

A flow chart in Figure 4 represents the processes involved in negative refractive index lens design using MATLAB software. Program codes were developed based on the equations and formula that were previously described in Sections 2.2.1 and 2.2.2. The initial parameters (n , θ_m , r_o , d_o) determined at the lens edge are shown in Figure 5. The equations for feed radiation pattern, $E_p^2(\theta)$, and aperture distributions, $E_d^2(x)$, are given. Next, differential Equations (1), (2) and (4) or (1), (2) and (9) are solved by the MATLAB routine of “ode45”.

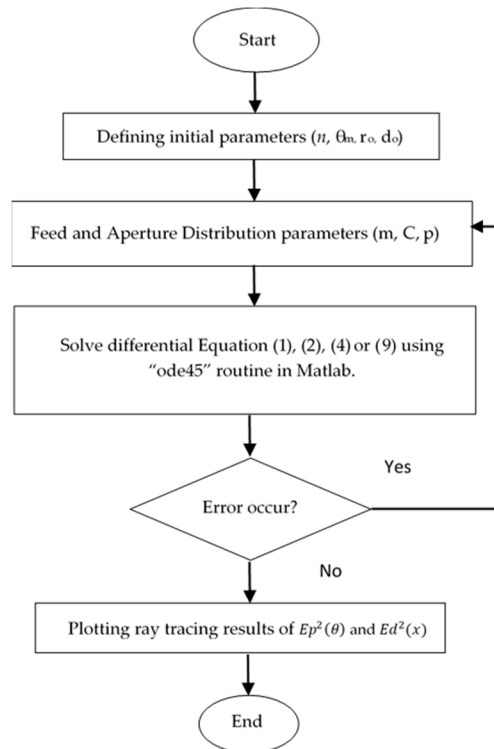


Figure 4. MATLAB Program.

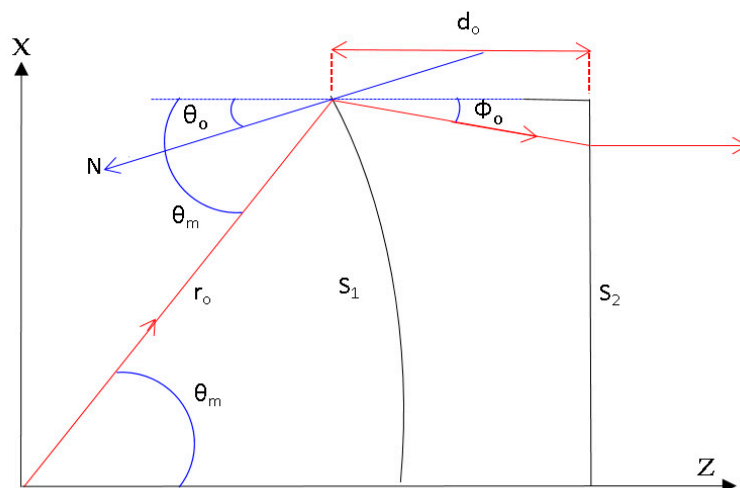


Figure 5. Initial parameters at the lens edge.

The explanation for the initial input values is shown in Figure 5. θ_o is an important parameter that determines the lens thickness where d_o is the initial thickness.

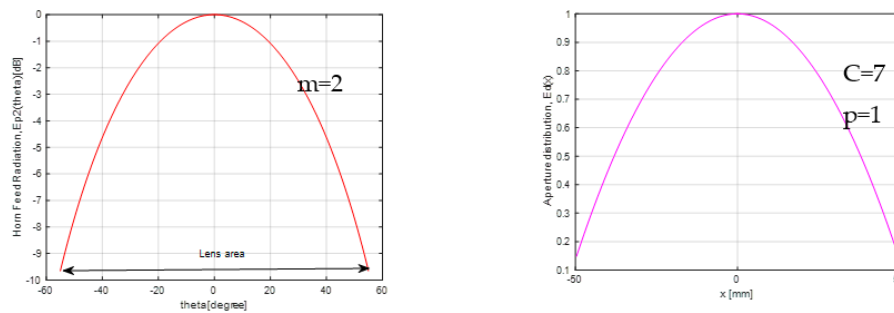
3. MATLAB Shape Design

3.1. Simulation of Energy Conservation Law

A negative refractive index lens is designed based on the energy conservation law by using Equations (3) and (4) in the MATLAB shape design program.

3.1.1. Aperture Distribution Design

Figure 6a shows the horn feed radiation, $Ep^2(\theta)$. The lens area is about -55° to 55° at -10 dB. It means that the area that is covered by the horn radiation beam is from -55° to 55° . The aperture distribution, $Ed^2(x)$, is shown in Figure 6b, which represents the edge level of the aperture distribution.



(a) Horn Radiation, $Ep^2(\theta)$

(b) Aperture Distribution, $Ed^2(x)$

Figure 6. Energy conservation design.

Aperture distribution can be expressed as in (10). When Equation (10) is compared with theoretical Equation (6) in Figure 7, it is observed that both equations have a good agreement with each other.

$$Ed^2(x) = \frac{d\theta}{dx} Ep^2(\theta) \tag{10}$$

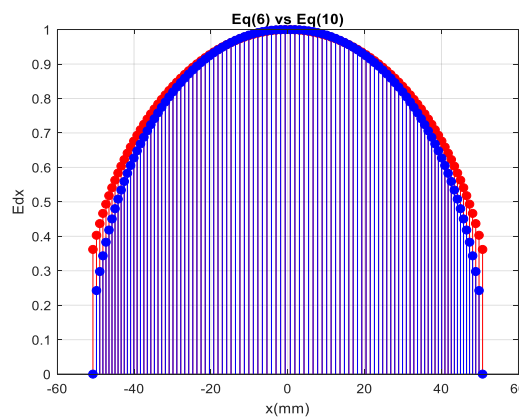


Figure 7. Comparison of aperture distribution.

Considering all the design parameters stated previously, the shaped lens was obtained as illustrated in Figure 8. For the designed lens in Figure 8, the accuracy of the MATLAB program was validated by calculating the incident angle, θ_i and refracted angle, θ_r at each surface of the lens. The refractive index value, n , was manually determined using the Snell's Law in (10). The calculated n value is expected to be similar to the n value ($n = -\sqrt{2}$), which is used in the MATLAB design program. The lens parameters are tabulated in Table 2.

$$n_1 \sin \theta_i = n_2 \sin \theta_r \tag{11}$$

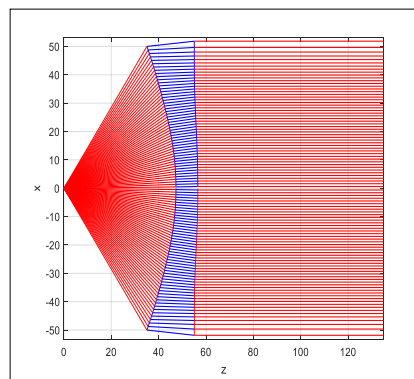


Figure 8. Shaped lens.

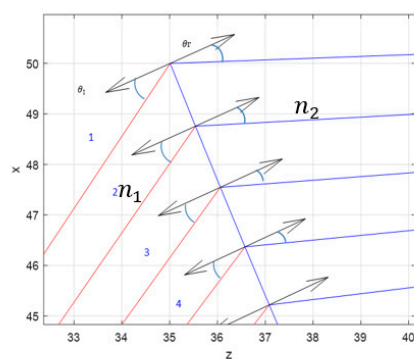
Table 2. Lens parameters.

Parameters	Value
Focal length (mm)	46.56
θ_m (°)	55
θ_o (°)	-24
n	$-\sqrt{2}$
C	7
d	20
Diameter (mm)	100

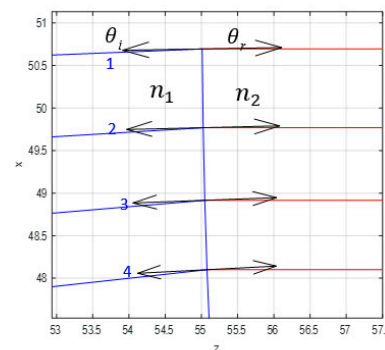
Table 3 represents the calculated n values considering the four first rays coming from the shaped lens in Figure 9a,b. The n_1 and n_2 values were calculated based on Equation (11) and compared to the exact n value that is used in MATLAB which is $n = -\sqrt{2}$. It is noticed that there is a small difference between the calculated values due to some errors that occurred during angle determination.

Table 3. Calculated n -value.

Ray in	θ_i (°)	θ_r (°)	n_2	Ray out	θ_i (°)	θ_r (°)	n_1
1	32	19	1.62	1	0.2	0.3	1.49
2	31	19	1.58	2	0.7	1.0	1.42
3	32	20	1.54	3	1.0	1.5	1.49
4	30	20	1.46	4	1.5	2.0	1.33



(a) Surface 1 (zoomed)



(b) Surface 2 (zoomed)

Figure 9. Rays in and rays out.

3.1.2. Abbe’s Sine Condition

The same process was repeated for Abbe’s sine Law by using Equations (7) and (9) in the MATLAB design program. The shaped lens is shown in Figure 10. The lens parameters are tabulated in Table 4.

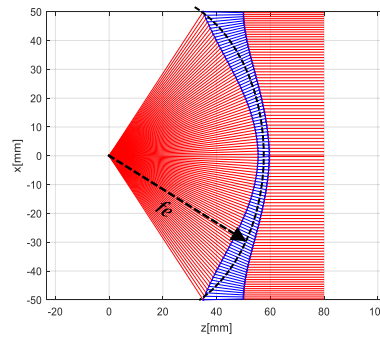
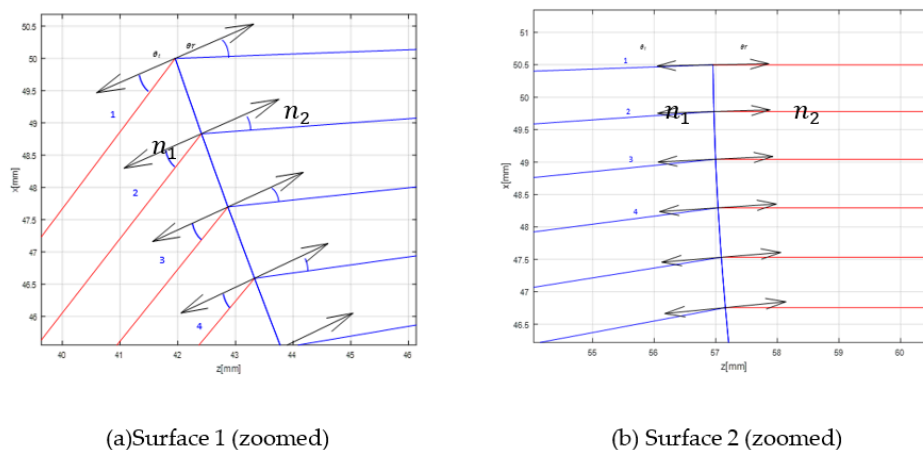


Figure 10. Abbe’s sine shaped lens.

Table 4. Lens parameters.

Parameters	Value
f_e (mm)	56.62
θ_m (°)	55
θ_o (°)	-24
n	$-\sqrt{2}$
C	7
d	15
Diameter (mm)	100

Table 5 represents the calculated n value considering the four first rays from the shaped lens in Figure 11a,b. A small difference between the calculated values and the exact value used in MATLAB may be due to errors during angle determination.



(a)Surface 1 (zoomed)

(b) Surface 2 (zoomed)

Figure 11. Rays in and rays out.

Table 5. Calculated n -value.

Ray in	θ_i (°)	θ_r (°)	n_2	Ray out	θ_i (°)	θ_r (°)	n_1
1	28	21	1.31	1	0.8	1	1.25
2	27	19	1.39	2	1.6	2	1.25
3	25	17	1.45	3	2	3	1.50
4	24	15	1.57	4	3	4	1.33

4. EM Simulations for Radiation Characteristics

4.1. Horn Feed

In order to calculate a negative refractive index material, the HFSS Simulator was used. In MATLAB, a point source was used to represent the feed, but in HFSS, a horn antenna was used to represent the feed radiator. Table 6 shows the simulation parameters using HFSS.

Table 6. Simulation parameters using High Frequency Structure Simulator (HFSS).

Parameters	Description/Value
Boundary Condition	Radiation Boundary
Refractive index, Permittivity, ϵ_r	$-1.4142 (\sqrt{-2} * \sqrt{-1})$
Permeability, μ_r	-2
	-1

A conical horn antenna is designed to operate at 28 GHz as shown in Figure 12a with the radiation pattern illustrated in Figure 12b.

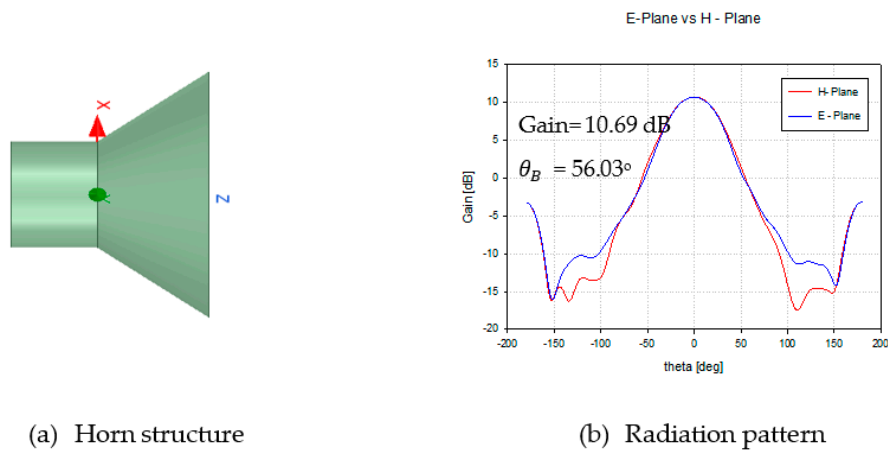


Figure 12. Performance of horn antenna as a feed radiator.

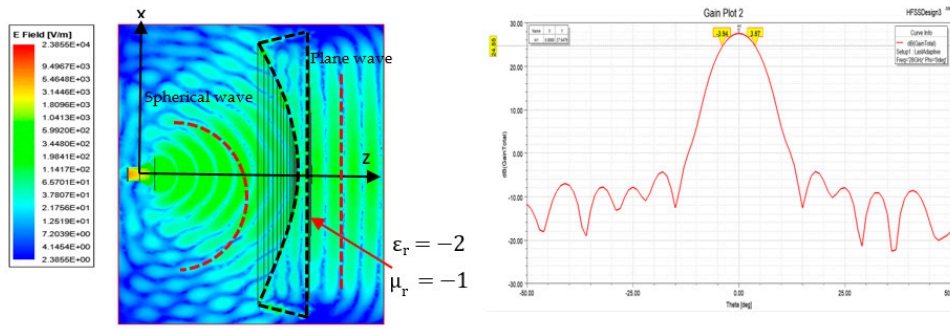
4.2. Energy Conservation Law

4.2.1. On-Focus

The designed shaped lens structure was simulated for performance evaluation. The lens structure has a permittivity of $\epsilon_r = -2$ and permeability $\mu_r = -1$. Figure 13a,b show the electric field distribution and the antenna gain, respectively. From Figure 13a, it is observed that the lens transformed the spherical wave into the plane wave. The obtained parameters are shown in Table 7. The theoretical value shows the uniform aperture case. This lens antenna structure produced a 27.55 dB gain with a beamwidth of 7.81° . The efficiency of the structure is about 66%.

Table 7. Lens structure simulation result.

	Theoretical	Simulation
Gain (dB)	29.35	27.55
θ_B ($^\circ$)	8.01	7.81
ΔG (dB)	0	-1.80
η (%)	100	66



(a) Electric Field (b) Antenna Gain

Figure 13. Energy conservation shaped lens performance.

4.2.2. Off-Focus

In order to prove that the designed lens shape is suitable for wide-angle beam scanning, multibeam characteristics are investigated in this paper. The feed horn position shifts spherically by 10° using the formula of $F = fs$, where F is the distance between the feed position and the center of the lens, while fs is the focal length. The off-focus position is illustrated in Figure 14.

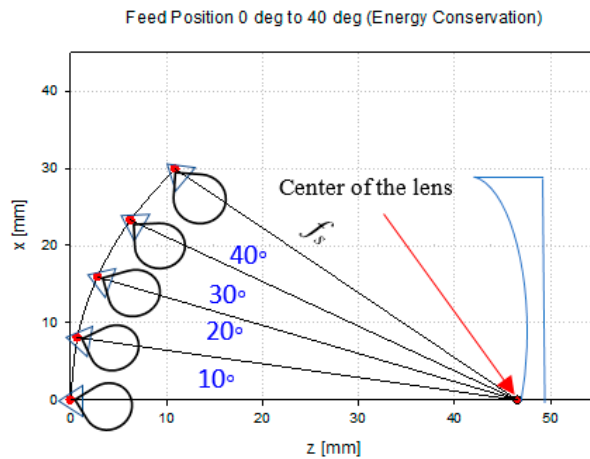


Figure 14. Feed position arrangement.

The results of antenna gain for different feed positions is illustrated in Figure 15 and Table 8. It is observed from the graph that there is no significant gain reduction for all the scanning angles. The scanning losses are all less than 3 dB, which indicates that beamwidths are consistent for all scanning angles. It can be concluded that this structure is suitable for wide-angle beam scanning.

Table 8. Simulation results of multibeam.

θ (°)	Gain (dB)	θ_B (°)
0	27.55	7.81
10	27.14	7.72
20	26.50	8.31
30	25.18	8.97
40	23.09	9.06

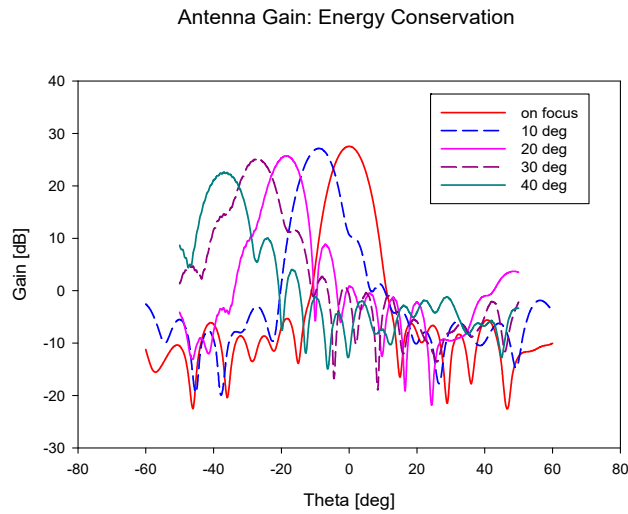


Figure 15. Antenna gain for scanning angle 0° to 40°.

Figures 16 and 17 show the results of the electric distribution in magnitude and phase, respectively, performed through near-field calculation. For on-focus condition, both intensity and phase distributions show uniform and symmetrical characteristics as shown in Figures 16a and 17a, respectively. In off-focus condition, the uniform characteristics are expected to be disturbed by some distortions due to the non-linearity in phase; thus, the behaviors are non-symmetrical, as observed in Figures 16b and 17b. Both electrical intensity and phase are slightly distorted when the feed is displaced from its original position.

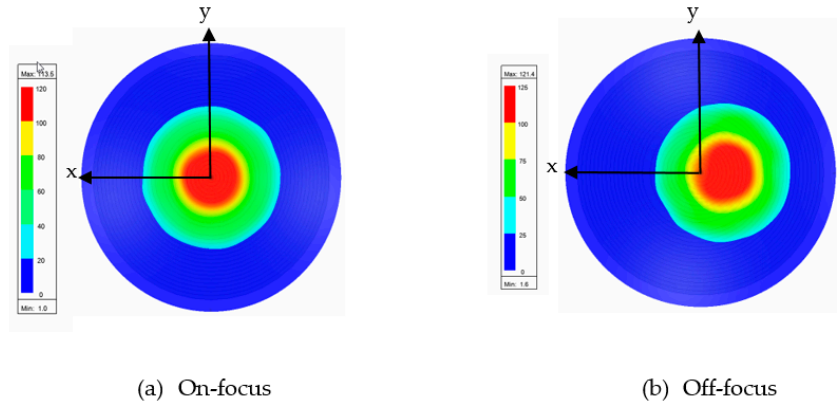


Figure 16. Electric intensity distribution.

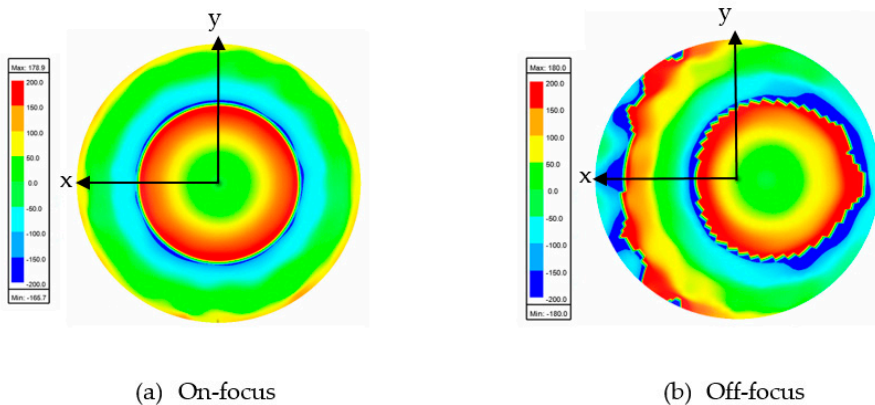


Figure 17. Electric phase distribution.

4.3. Abbe's Sine Law

4.3.1. On-Focus

For Abbe's sine condition, a shaped lens structure with the permittivity value of $\epsilon_r = -2$ and permeability value of $\mu_r = -1$ was simulated as shown in Figure 18a. The performance of the designed lens is illustrated in Figure 18b. It is observed that this Abbe's sine shaped lens produced a gain of 27.48 dB. The beamwidth is 7.64° . This lens also has 65% efficiency, as shown in Table 9.

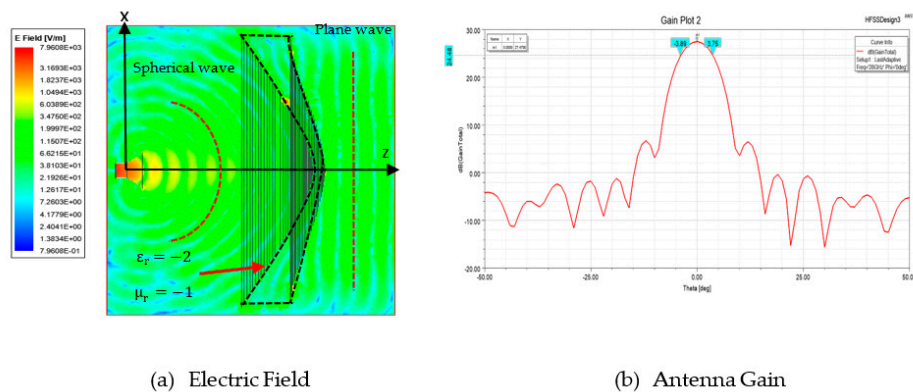


Figure 18. Abbe's sine shaped lens performance.

Table 9. Simulation results.

	Theoretical	Simulation
Gain (dB)	29.35	27.48
θ_B ($^\circ$)	8.01	7.64
ΔG (dB)	0	-1.87
η (%)	100	65

4.3.2. Off-Focus

For multibeam investigation, the feed position of the horn antenna is varied from 0° to 40° with 10° intervals as illustrated in Figure 19. The same condition in energy conservation ($F = fs$) was applied for Abbe's sine shaped lens. The results for all scanning angles are represented in Figure 20 and Table 10. The gain is slightly lower as compared to the energy conservation shaped lens. However, there is no significant gain reduction for every scanning angle. The beamwidths are also consistent for all scanning angles.

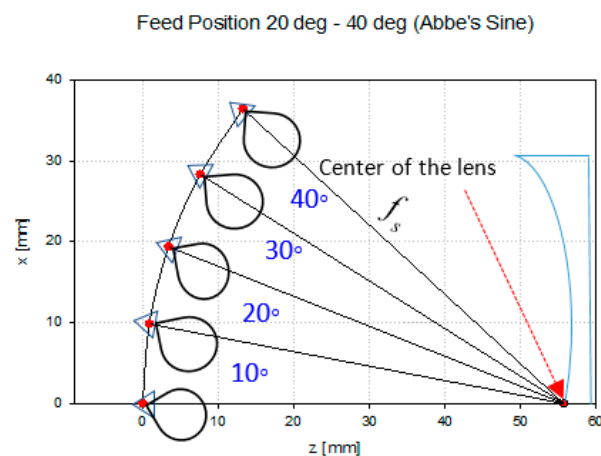


Figure 19. Feed position arrangement.

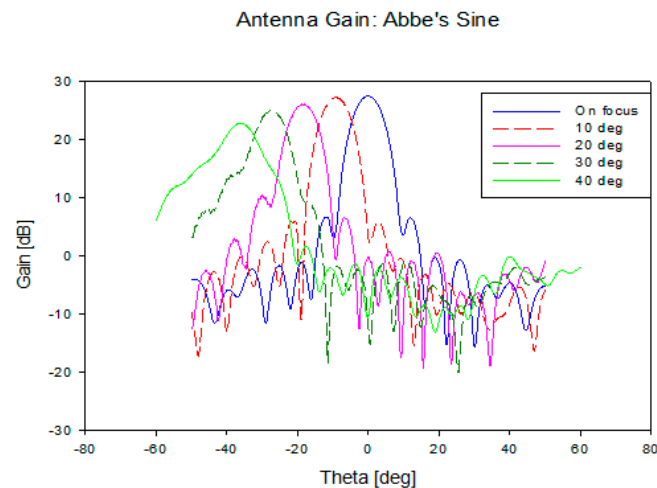


Figure 20. Antenna gain for scanning angle 0° to 40° .

Table 10. Simulation results of different feed positions.

θ ($^\circ$)	Gain (dB)	θ_B ($^\circ$)
0	27.48	7.64
10	27.19	7.37
20	26.73	8.08
30	25.54	8.43
40	22.92	9.43

Figure 21a,b show the results of the electric field distribution during off-focus for Energy Conservation and Abbe's sine lens, respectively.

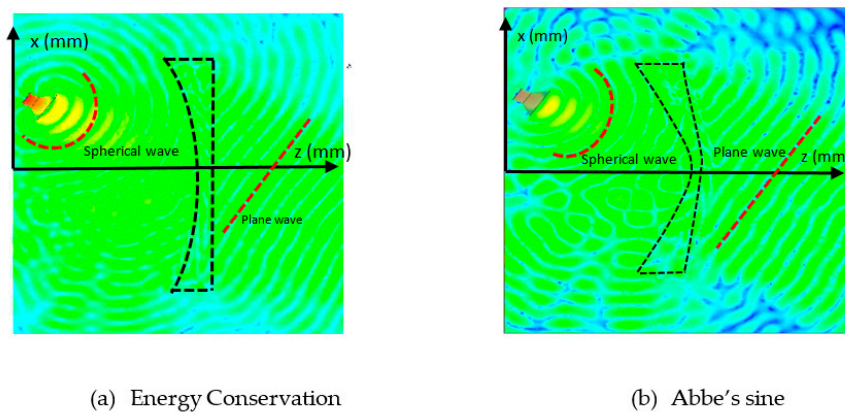


Figure 21. Electric field distribution during off-focus.

Figures 22 and 23 show the results of the electric distribution in magnitude and phase, respectively, for Abbe's sine lens. For on-focus condition, both intensity and phase distributions exhibited uniform characteristics as shown in Figures 22a and 23a, respectively. Figures 22b and 23b present off-focus condition, which shows that both electrical intensity and phase are slightly distorted. The feed displacement from its original position affects the electrical intensity and the phase distribution linearity.

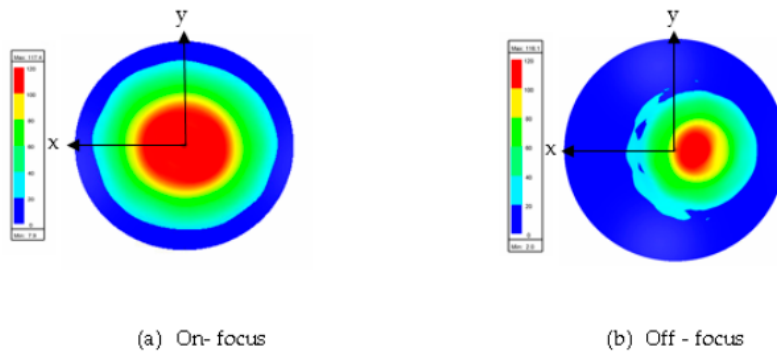


Figure 22. Electric intensity distribution.

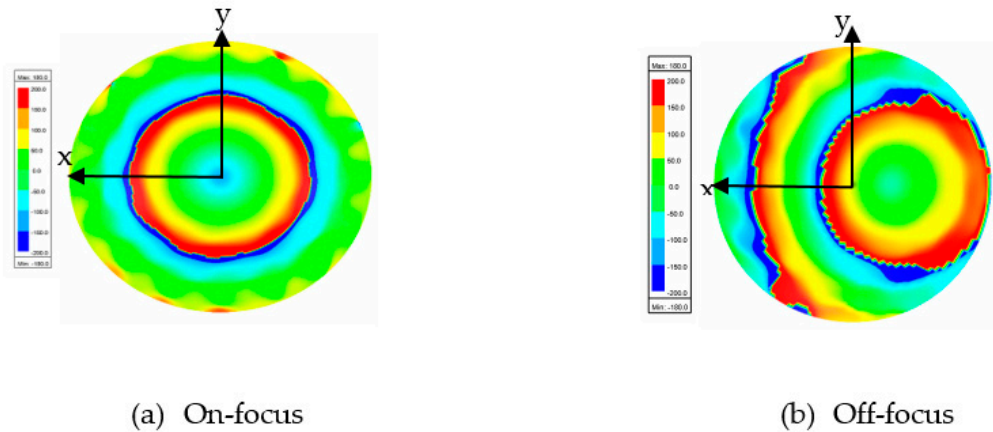


Figure 23. Electric phase distribution.

The performance for both types of lens are compared in Figure 24a,b. In terms of gain and beamwidth, the performances of both lenses are similar: there is not much difference, as shown in Figure 24a below.

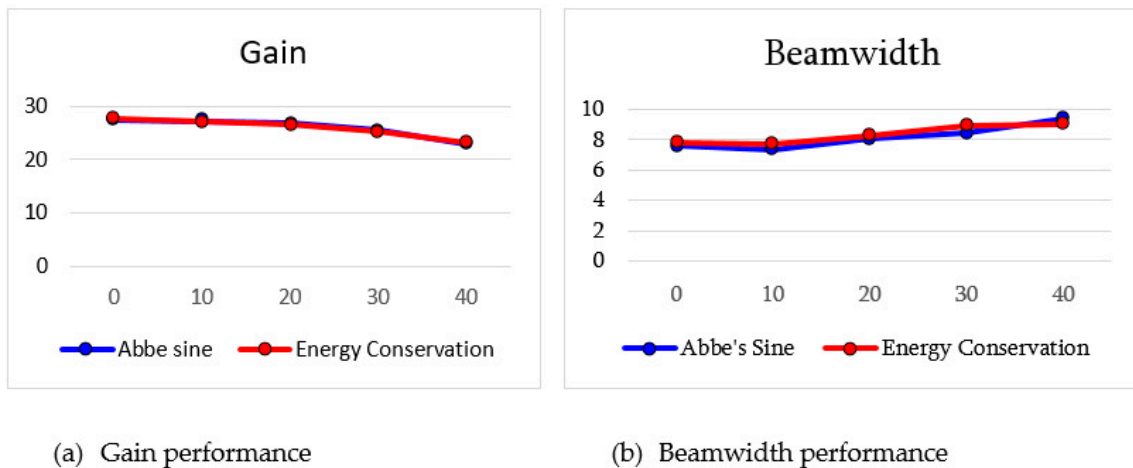


Figure 24. Performance comparison for both types of lens.

4.4. Feed Position Analysis

In this section, the performance of the feed position for scanning angles of 20° until 40° is analyzed. The performance of the designed energy conservation lens and Abbe's sine lens is evaluated when the feed is located closer and farther from the lens. The original position is $F = fs$ as shown in Figure 25. θ is the scanning angle which is varied from 20° to 40°. The original position is the calculated position

based on the shaped lens. Position 2 is where the feed is placed farther from the lens, while position 3 is where the feed is placed closer to the lens.

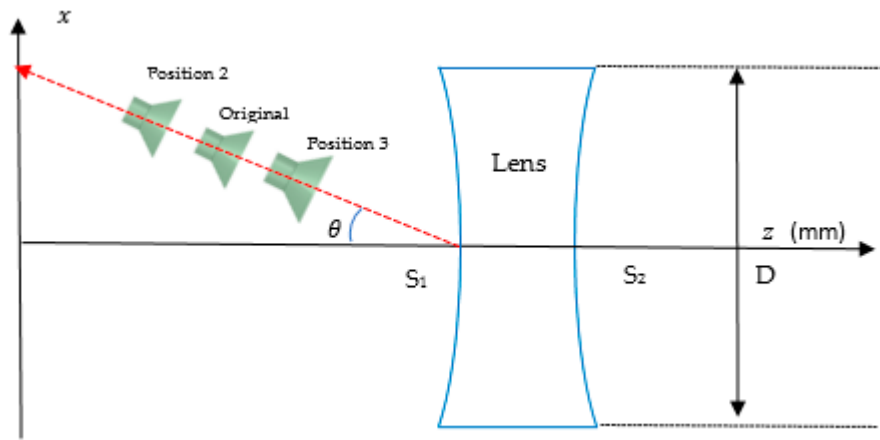


Figure 25. Feed position analysis arrangement.

Figures 26 and 27 show the performance of the designed energy conservation lens and Abbe’s sine lens antenna for all feed positions from 20° to 40° scanning angle, respectively. At each scanning angle, there is no significant difference in gain, beamwidth and shift angle between the three feed positions. It can be seen that these two types of designed lens perform consistently for all the feed positions.

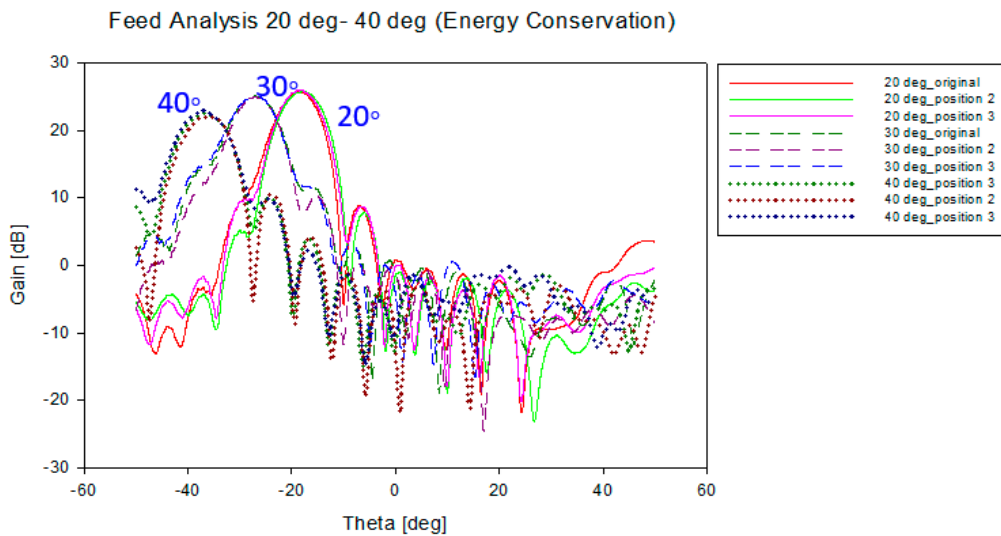


Figure 26. Antenna gain for all feed position for energy conservation lens.

Table 11 shows the overall performance for both types of lens at 20° , 30° and 40° scanning angle. From all the results shown in Figure 26, Figure 27 and Table 11, it can be seen that all the positions along the lines satisfied the $F = fs$ condition with optimum performance. It shows that the $F = fs$ condition and both lens structures are suitable for multibeam applications. Hence, this structure can be applied for 5G mobile base station.

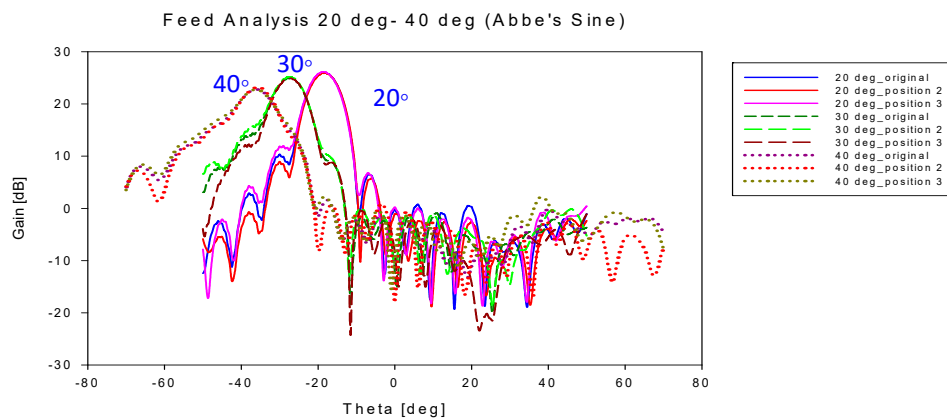


Figure 27. Antenna gain for all feed position for Abbe's sine lens.

Table 11. Performance for all positions at 20°, 30° and 40° scanning angle.

θ	Position	Focal Length (mm)		Gain (dB)		Beam Width (°)		SLL (dB)		Shift Angle (°)	
		Energy	Abbe	Energy	Abbe	Energy	Abbe	Energy	Abbe	Energy	Abbe
20	Original	46.56	56.62	26.50	26.73	8.31	8.08	-17.15	-17.95	-18	-18
	Position 2	48.68	58.74	26.12	26.55	8.36	7.95	-16.63	-17.93	-17	-18
	Position 3	44.44	54.50	26.93	26.66	7.99	8.08	-16.39	-15.93	-17	-18
30	Original	46.56	56.62	25.18	25.54	8.97	8.43	-11.65	-11.37	-25	-27
	Position 2	48.68	58.74	24.92	25.25	8.95	8.50	-11.60	-11.36	-25	-27
	Position 3	44.44	54.50	25.57	25.39	9.02	8.66	-12.24	-11.53	-26	-27
40	Original	46.56	56.62	22.61	22.78	9.48	9.34	-8.05	-7.22	-37	-36
	Position 2	48.68	58.74	22.13	23.18	9.50	9.20	-5.98	-7.94	-37	-36
	Position 3	44.44	54.50	22.92	22.73	9.61	9.41	-6.68	-7.81	-37	-36

5. Conclusions

Two types of negative refractive indexes lens were designed in MATLAB software and simulated by using the electromagnetic simulator ANSYS HFSS. Both the energy conservation lens and Abbe's sine lens offer high gain and narrow beam width characteristics with 66% and 65% efficiency, respectively. A 27.55 dB maximum gain is achieved for the energy conservation lens and 27.48 dB for Abbe's sine lens. Moreover, both shaped lenses provide optimum results for beam scanning up until 40°. High gain, narrow beam width and wide-angle beam scanning capability are the key elements for 5G application. Thus, it can be concluded that these two types of refractive index lens are good candidates for 5G mobile base station application.

Author Contributions: Conceptualization, Y.Y.; Funding acquisition, D.N.Q.; Software, P.V.H.; Supervision, N.H.A.R. and Y.Y.; Validation, Y.Y.; Writing—original draft, S.A.H.; Writing—review & editing, N.H.A.R., Y.Y. and D.N.Q. All authors have read and agreed to the published version of the manuscript.

Funding: The work by Nguyen Quoc Dinh and Phan Van Hung is funded by Vietnam National Foundation for Science and Technology Development (NAFOSTED) under grant number 102.04-2018.08. The work by Salbiah, Nurul Huda and Yoshihide Yamada is funded by Malaysia Ministry of Higher Education under grant number FRGS/1/2018/TK04/UITM/03/5.

Acknowledgments: Authors would also like to acknowledge Antenna Research Centre, Faculty of Electrical Engineering, Universiti Teknologi MARA and Malaysia-Japan International Institute of Technology, Universiti Teknologi Malaysia for supporting this project.

Conflicts of Interest: The authors declare no conflict of interest.

References

1. Stutzman, W.L.; Thiele, G.A. Aperture Antenna. In *Antenna Theory and Design*, 3rd ed.; Ashenberg, W., Ed.; John Wiley & Sons, Inc.: Hoboken, NJ, USA, 2012; Volume 1, pp. 344–428.
2. Lee, J.J. Lens Antenna. In *Antenna Theory*, 1st ed.; Lo, Y.T., Lee, S.W., Eds.; Van Nostrand Reinhold: New York, NY, USA, 1993; Volume 2, pp. 5–58.

3. Milligan, T.A. Lens antenna. In *Modern Antenna Design*, 2nd ed.; John Wiley & Sons, Inc.: Hoboken, NJ, USA, 2005; Volume 1, pp. 447–451.
4. Matytsine, L.; Lagoiski, P.; Matytsine, M.; Matitsine, S. Large Size, Lightweight, Luneburg Lenses for Multi-beam Antenna Applications. In Proceedings of the 6th European Conference on Antennas and Propagation (EUCAP), Prague, Czech Republic, 26–30 March 2012.
5. Liu, K.; Yang, S.; Qu, S.; Chen, Y. A Flat Luneberg Lens Antenna for Wide-Angle Beam Scanning. In Proceedings of the IEEE International Symposium on Antennas and Propagation and USNC-URSI Radio Science Meeting, Atlanta, GA, USA, 7–12 July 2019.
6. Christopher, C.; Tatsuo, I. *Electromagnetic Metamaterial: Transmission Line Theory and Microwave Application*; John Wiley & Son: Hoboken, NJ, USA, 2006; Chapter 7; pp. 316–322.
7. Thorton, J.; Huang, K.-C. *Modern Lens Antenna for Communications Engineering*; IEEE Press: Piscataway, NJ, USA, 2013; pp. 29–30.
8. Kamada, S.; Michishita, N.; Yamada, Y. Metamaterial lens antenna using dielectric resonator for wide angle beam scanning. In Proceedings of the IEEE Antennas and Propagation society international symposium (APSURSI), Toronto, ON, Canada, 11–17 July 2010; pp. 1–4.
9. Samuel Silver. *Microwave Antenna Theory and Design*; McGrawhill: New York, NY, USA, 1949; p. 394.



© 2020 by the authors. Licensee MDPI, Basel, Switzerland. This article is an open access article distributed under the terms and conditions of the Creative Commons Attribution (CC BY) license (<http://creativecommons.org/licenses/by/4.0/>).